Source Characteristics of the M_w 6.2 Loreto Earthquake of 12 March 2003 that Occurred in a Transform Fault in the Middle of the Gulf of California, Mexico

by Leobardo López-Pineda and Cecilio J. Rebollar

Abstract   We analyzed the Loreto earthquake of 12 March 2003 M_w 6.2, which occurred in the transform fault that joins the Guaymas and Carmen Basins in the middle of the Gulf of California. This event was recorded by a network of autonomous continuously recording broadband seismographs located over the Baja California Peninsula, Sonora, and Sinaloa states of Mexico. The main event was located at 26.615° N and 111.09° W, at a depth of 5.0 ± 2 km. A foreshock of magnitude 4.2 was recorded and located at 26.580° N and 111.011° W. We located 35 aftershocks, 20% of them were located in the rupture area of the mainshock consistent with a nearly vertical right-lateral strike-slip fault with a northwest–southeast trend. Rupture propagation derived from waveform analysis indicated that the rupture propagated from northwest to southeast. Most of the aftershocks occurred southeaster of the main event. From the statistical analysis of 333 aftershocks we calculated a b-value of 0.68.

Focal depth and fault geometry were estimated from body-wave form modeling of P and S waves. Synthetics were calculated using Herrmann's (1987) reflectivity code with a triangular source time function of 6 sec. The best match between synthetics and recorded P and S waves were obtained with a fault geometry given by a strike of 117° ± 4°, a dip of 79° ± 2°, and a slip of 168° ± 2°. We calculated a seismic moment of 2.68×10^{18} N m (2.68×10^{25} dyne cm), a source radius of 6.8 ± 0.7 km, and a static stress drop of 3.8 ± 1.2 Mp (38 ± 12 bars). Calculated static stress drops of previous events located in the Gulf of California range from 0.2 to 12.5 Mp (2 to 125 bars).

Introduction

Centro de Investigación Científica y de Educación Superior de Ensenada (CICESE) deployed two broadband seismic stations in 1995 at Bahia de los Angeles (Baja California) and Guaymas (Sonora). Later, those stations were increased to a total of eight broadband stations to conform to what we called Red Sismologica de Banda Ancha (RESBAN). This network was recently complemented with the NARS-Baja network that consists of 14 broadband seismic stations from Utrecht University (The Netherlands), in a joint project between Utrecht University, California Institute of Technology, and CICESE (Trampert *et al.*, 2003). Up to now this network consisted of 23 broadband seismic stations located in the Peninsula of Baja California, Sonora, and Sinaloa states of Mexico (Fig. 1). The purpose of this network is to study local and regional seismicity and the crust and upper-mantle structure.

The earthquake of 12 March 2003 M_w 6.2 is the first earthquake with a magnitude greater than 6 recorded by nearby seismic stations. Initially, it was located at 26.3° N and 110.6° W at a depth of 10 km by the National Earthquake Information Center (NEIC), 80 km southeast of Loreto where the NE77 seismic station is located. This event was recorded by nearby broadband, continuously recording digital seismic stations, mainly, NE77, NE76, NE78, NE82, and GUAY. These stations constrained the earthquake location (see Fig. 2). The recorded sequence was foreshock-mainshock-aftershock.

The middle of the Gulf of California is characterized by the presence of oceanic basins (pull-apart) connected by transform en echelon faults following a northwest–southeast strike (Lonsdale, 1989). In the present study, we define the active segment of the transform fault between the Guaymas and Carmen basins where the Loreto earthquake occurred. We also report source parameters, fault geometry, b-value, and location of the foreshock, mainshock, and 35 aftershocks with magnitudes up to 3.5 that occurred during the next two
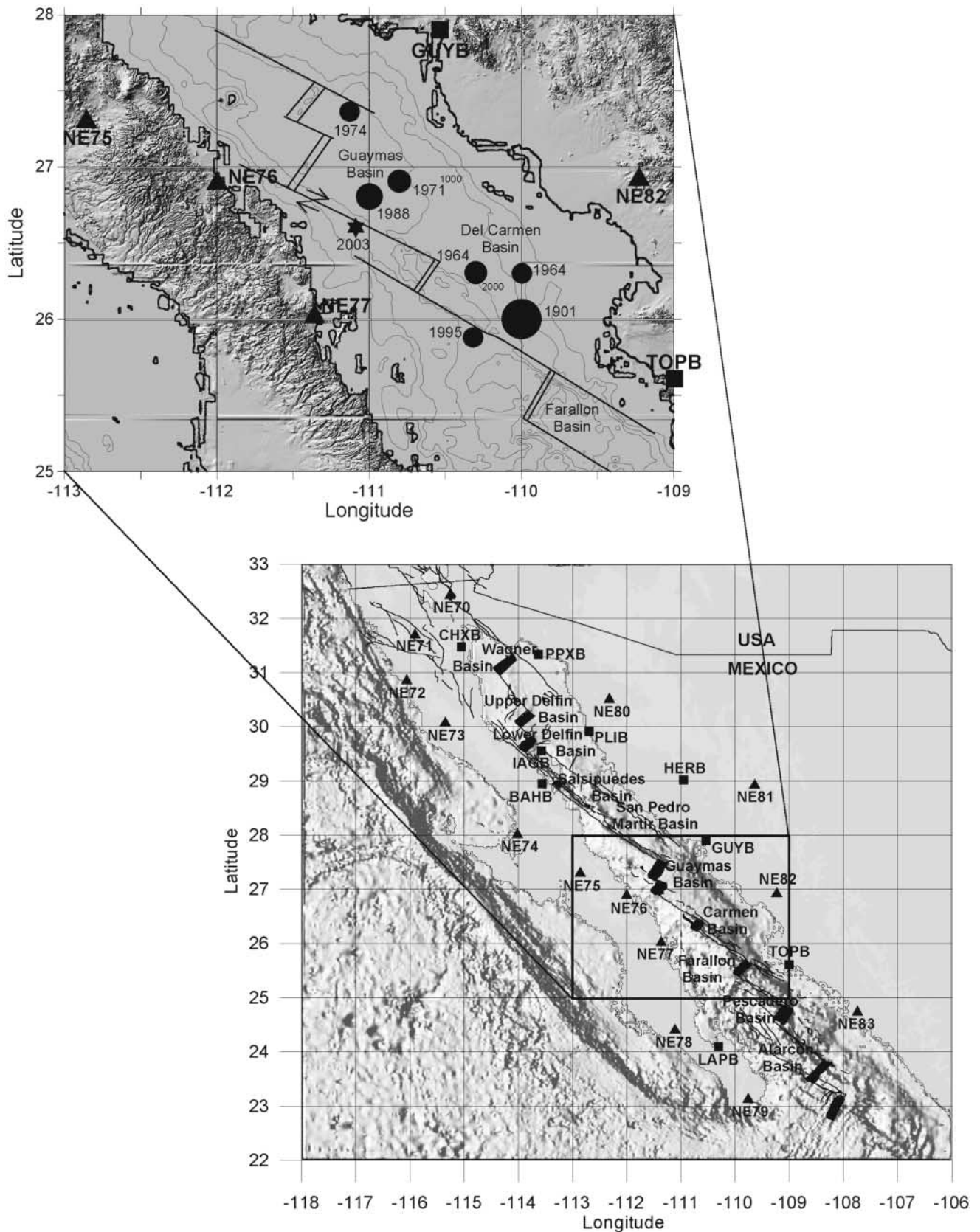
Figure 1.   Lower map shows the location of the broadband seismic stations (triangles) and the basins of the Gulf of California. Upper inset shows the location of the twentieth-century earthquakes (circles) and the location of the Loreto earthquake (star). Magnitudes of the earthquakes are related to the size of the circles. Also shown from northwest to southeast are the Guaymas, Carmen, and Farallon basins. Continuous lines are the inferred transform faults from Lomnitz et al. (1970) and Lonsdale (1989).
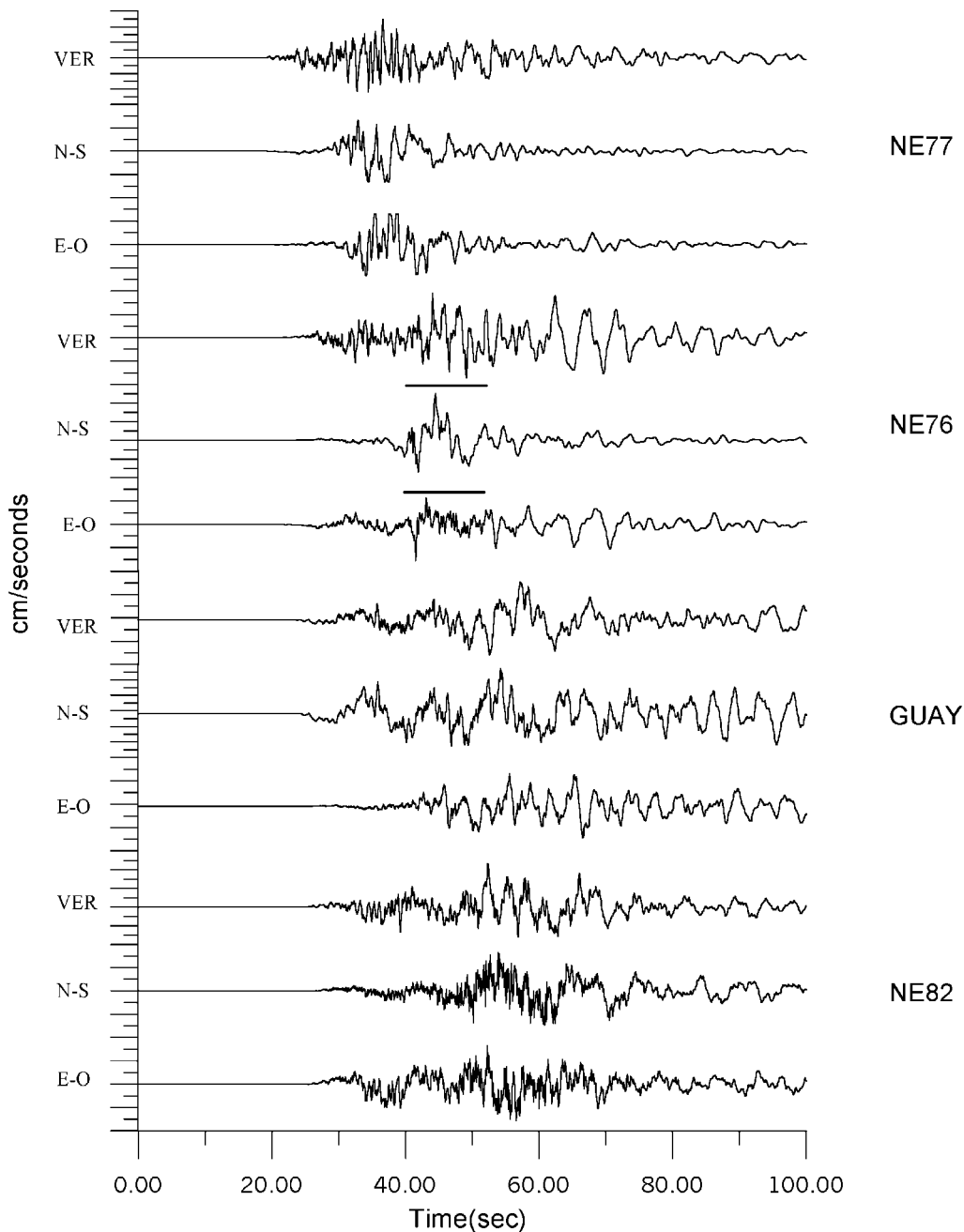
Figure 2. Plot of the seismograms recorded by the NE77, NE76, GUAY, and NE82 seismic stations. The upper bars at the horizontal components of the NE76 seismic station are the time windows used in the calculation of the Fourier spectra. The horizontal components of the surface waves recorded at NE77 seismic station are clipped.

days. We compare the source characteristics of this event with the events that have occurred in the Gulf of California.

Tectonic and Historical Seismicity

The middle sector of the Gulf of California is part of the boundary between the North American and Pacific Plates. This sector is located in the Gulf of California Extensional Province; it comprises the following pull-apart basins: Guaymas Basin, Carmen Basin, and Farallon Basin, all linked by inferred transform faults with a northwest–southeast strike (Lonsdale, 1989) (Fig. 1).

The basins in the middle of the Gulf of California are different from those located in the mouth of the Gulf of California, because they have developed magnetic anomalies in contrast with those located in the head of the Gulf of California that are dominated by a pull-apart regimen and a steady thinning of the continental crust. Carmen Basin has

Table 1

Earthquakes with Magnitude Greater than 6 That Have Occurred
in the Neighborhood of the Carmen Basin

Zone Carmen Basin	Date (yyyy/mm/dd)	Latitude (° N)	Longitude (° W)	Seismic Moment (N m)	Magnitude M_w
South	1901/01/07*	26.00	110.00	44.0×10^{18}	7.0
	1964/07/05[†]	26.30	110.00	4.0×10^{18}	6.3
	1964/07/06[†]	26.30	110.30	7.8×10^{18}	6.5
	1995/08/28[‡]	25.88	110.32	3.0×10^{18}	6.2
North	1971/09/30[†]	26.90	110.80	6.7×10^{18}	6.5
	1974/05/31[†]	27.36	111.13	3.8×10^{18}	6.3
	1988/02/24*	26.80	111.00	11.0×10^{18}	6.6
	2003/03/12[§]	26.53	111.09	2.68×10^{18}	6.2

*Pacheco and Sykes (1992).
[†]Goff *et al.* (1987).
[‡]Tanioka and Ruff (1997).
[§]This study.

Table 2

One-dimensional Crustal Velocity Model Used to Calculate the
Synthetic Seismograms and to Locate the Loreto Earthquake
(Rebollar *et al.*, 2001)

Layer Thickness (km)	*P*-wave velocity (km/sec)	*S*-wave velocity (km/sec)	Density (g/cm³)	Q_α	Q_β
4.0	4.0	2.6	2.3	400	200
4.0	5.7	3.3	2.5	2000	2000
16.0	6.7	3.8	3.0	2000	2000
0.0	7.8	4.0	3.4	2000	2000

a magnetic anomaly that suggests a spreading velocity from 2 to 6 cm/year (Larson *et al.*, 1972).

Pacheco and Sykes (1992) reported a catalog of events (worldwide) greater than 7 from the nineteenth century up to 1988. They report an event that occurred in 1901 of mag-
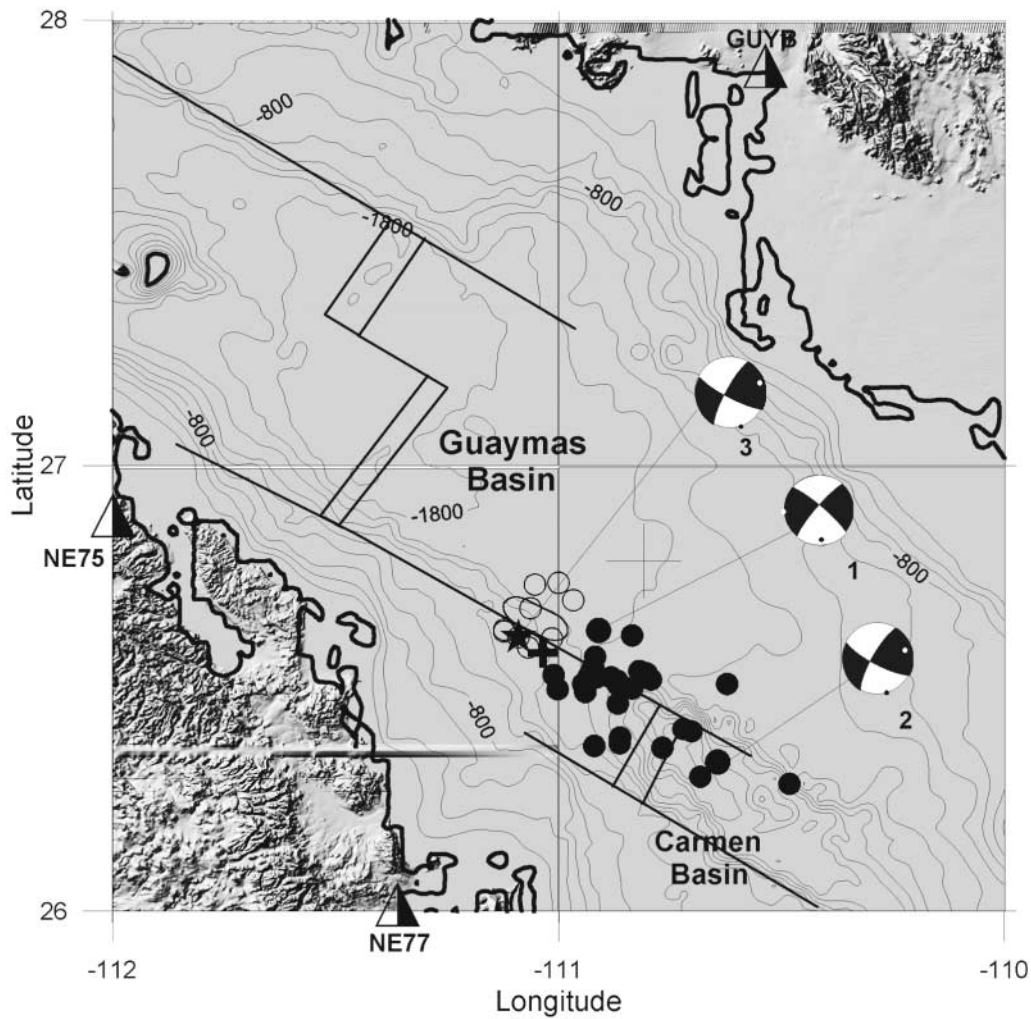

Figure 3.   Map showing the location of the Loreto earthquake (star), a foreshock (cross), and its aftershocks (open circles). Filled circles are aftershocks triggered by the main event. The ellipse shows the rupture area inferred from the Brune circular fault model. Half-filled triangles are the seismic stations. Also shown are the fault plane solution reported by Harvard (1) and NEIC (2). Our fault plane solution is 3.

nitude 7.0 south of Carmen Basin. On the other hand, Goff *et al.* (1987) reported the source parameters of the events of 5 and 6 July 1964, magnitudes 6.3 and 6.5; and Tanioka and Ruff (1997) reported the source time function of the 28 August 1995 magnitude 6.2 event that occurred southeast of Carmen Basin. The events of 24 February 1988, magnitude 6.6, 30 September 1971, magnitude 6.5, and 31 May 1974, magnitude 6.3, and the Loreto earthquake occurred northwest of Carmen Basin (Table 1 and Fig. 1).

Data Recording

The NARS-Baja broadband station consists of an STS2 sensor, a 24-bit data logger, a Global Positioning System (GPS), and a laptop for data acquisition and timing (Trampert *et al.*, 2003). The RESBAN broadband station consists of a Guralp CMG-40T or CMG-3ESP sensors, 24-bit Guralp digitizers, GPS, and a CMG-SAM2 acquisition module. Every station is located in similar shelters to provide protection and, whenever possible, over outcrops. All seismic stations record continuously at 20 samples per second.

Earthquake Location

To locate the Loreto earthquake of 12 March 2003 we used the NE76, NE77, NE78, NE82, and GUYB stations, the closest stations to the epicenter. Figure 2 shows the seismograms. We used *P*- and *S*-wave picks at those stations and the crustal velocity model used by Rebollar *et al.* (2001) (Table 2) to locate the event with the HYPOCENTER code (Lienert *et al.*, 1988; Lienert and Havskov, 1995). The epicenter was well constrained at 26.615° N and 111.09° W with standard errors in latitude and longitude of the order of ±5.5 km (Fig. 2). The depth of the source was not well constrained with the HYPOCENTER code. The hypocenter, however, was estimated with the match of the observed and synthetic seismograms of the *S* waves observed at the NE77, NE76, and GUYB seismic stations at a depth of 5 ± 2 km. We also located a foreshock (M_w 4.2) at 26.530° N and 111.011° W and 35 aftershocks; seven of them are located over the rupture area of the mainshock, which suggests a fault with a northwest–southeast trend (Fig. 3). The Loreto earthquake occurred northwest of the transform fault between Guaymas and Carmen Basins, whereas most of the seismicity occurred southeast toward Carmen Basin, delineating an active segment of the transform fault of about 60 km in length (Fig. 3).

We calculated duration magnitudes of 333 aftershocks recorded at the NE77 seismic station using the expression given by M_D 2.24 $\log_{10} T - 0.85$, where *T* is the duration of the signal. This relationship was used by Rebollar and Riechle (1987) in the Northern Peninsular Ranges of Baja California and it is routinely used by Red Sismica del Noroeste de Mexico (RESNOM). Duration magnitudes of the located earthquakes range from 0.3 to 3.5 The *b*-value from

the Gutenberg-Richter relationship was calculated. The estimated *b*-value was 0.68 (Fig. 4). This low *b*-value suggests a homogeneous concentration of stresses according to Scholz (1968) in contrast with large *b*-values obtained in earthquake swarms that have occurred in the Gulf of California (Reichle and Reid, 1977).

P- and *S*-Wave Modeling

The NE77 seismic station lies 72 km south of the epicenter of the Loreto earthquake. Because of the orientation of the fault rupture, the NE77 seismic station recorded the main energy of the *SH* waves, and the amplitude of the surface waves were clipped. Before integration, seismic traces were corrected by instrument response to have velocity records in centimeters per sec. The integrated north–south and east–west components, without filtering, showed that the apparent source time function (ASTF) resembled a triangle with a duration of nearly 6.0 sec. Synthetic seismograms in a plane-layered elastic medium were calculated by using Herrmann's (1987) reflectivity code. We used the crustal velocity model reported by Rebollar *et al.* (2001) to calculate the synthetic seismograms of the Loreto earthquake. The purpose was to identify the mechanism that best fits 14 sec of the record at the NE77 seismic station, the unclipped section of the seismogram. The best match was obtained with a strike of 117° ± 4°, dip of 79° ± 2°, slip of 168° ± 2°, and a focal depth of 5 ± 2 km (Fig. 5). The errors are the range of variation of the parameters where the fit is equally good. This result, within the errors, agrees quite well with the fault geometry reported by NEIC and Harvard (Table 3). With this fault geometry we fitted 16 sec of the *P* and *S* waves at the NE76 and GUYB seismic stations (95 and 152 km away
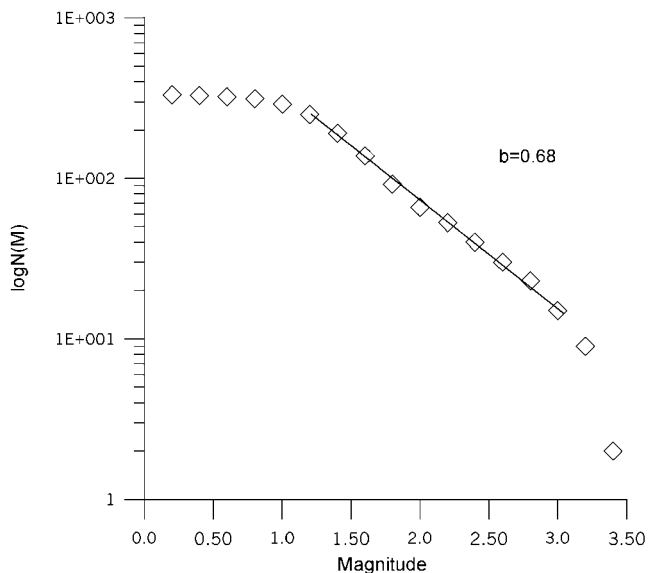

Figure 4. Frequency-magnitude plot of the aftershocks of the Loreto earthquake recorded at the NE77 seismic station. A *b*-value of 0.68 was calculated.
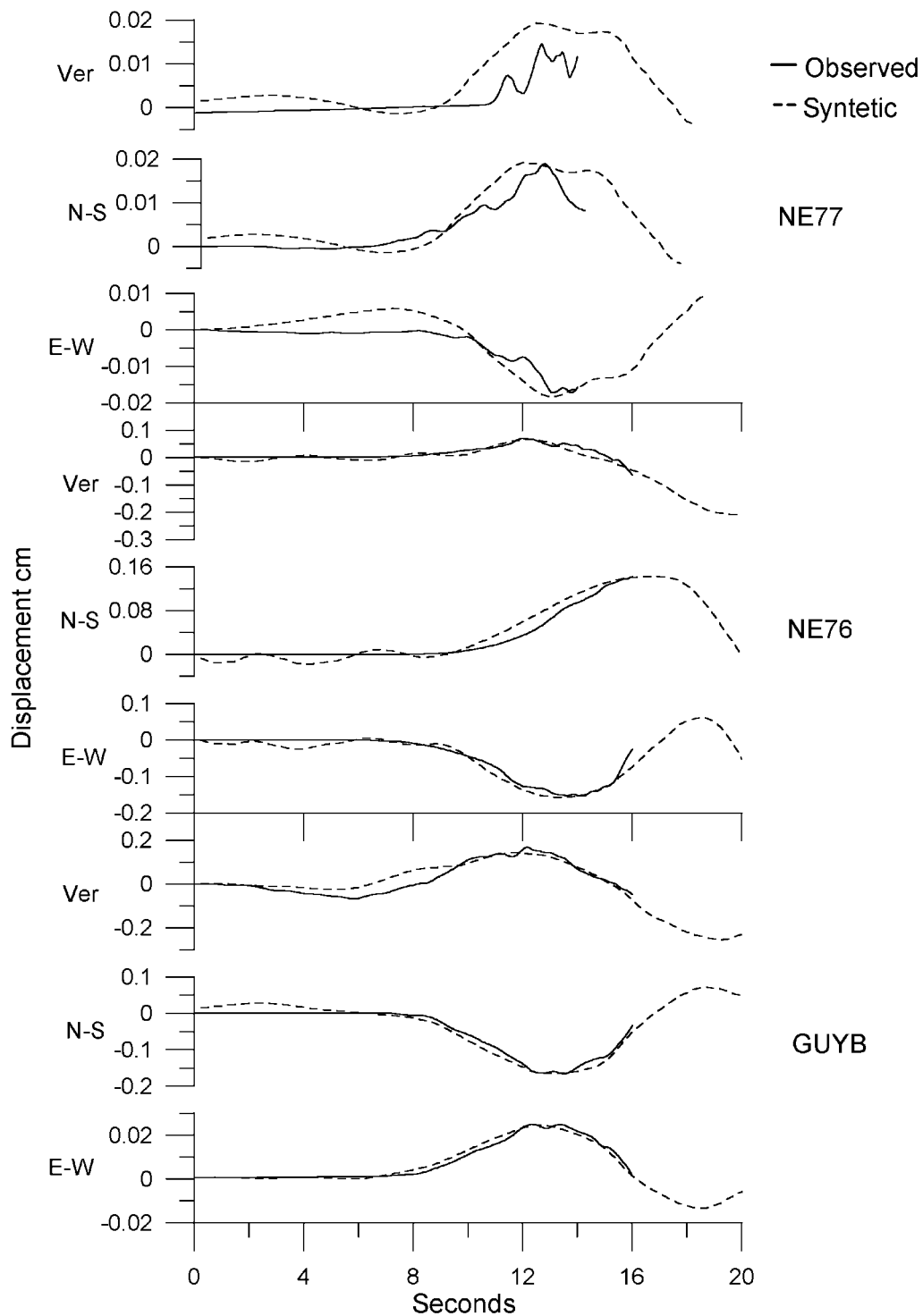
Figure 5.   Comparison of observed *P*- and *S*-wave amplitudes (continuous line) recorded at the NE77, NE76, and GUYB seismic stations with the synthetic seismograms (discontinuous line) calculated with the reflectivity method (Herrmann, 1987). Observed and synthetic seismograms of the NE77 seismic station were compared before the clipped amplitudes. The agreement is excellent.

from the epicenter, respectively) without filtering. The fit was excellent as seen in Figure 5.

To see the directivity, we isolated the ASTF recorded at the NE76 seismic station, located northwest of the fault, and the ASTF recorded at the NE82 seismic station located southeast of the fault. We filtered and rotated the ASTF using a bandpass Butterworth filter between 0.1 and 0.2 Hz. Afterward the ASTF values were normalized (Fig. 6). We found

that the ASTF is shorter at NE82 than the ASTF observed at NE76. This effect is more clearly seen in the radial component. Therefore, we can conclude that the rupture propagated from northwest to southeast.

We found similarities in the ASTFs and fault geometries of the foreshock and mainshock. First, we calculated the synthetic seismograms of the foreshock with the same fault geometry of the mainshock, but in this case we filtered the

Table 3
Earthquake Locations and Fault Geometry Calculated by CICESE, Harvard, and NEIC

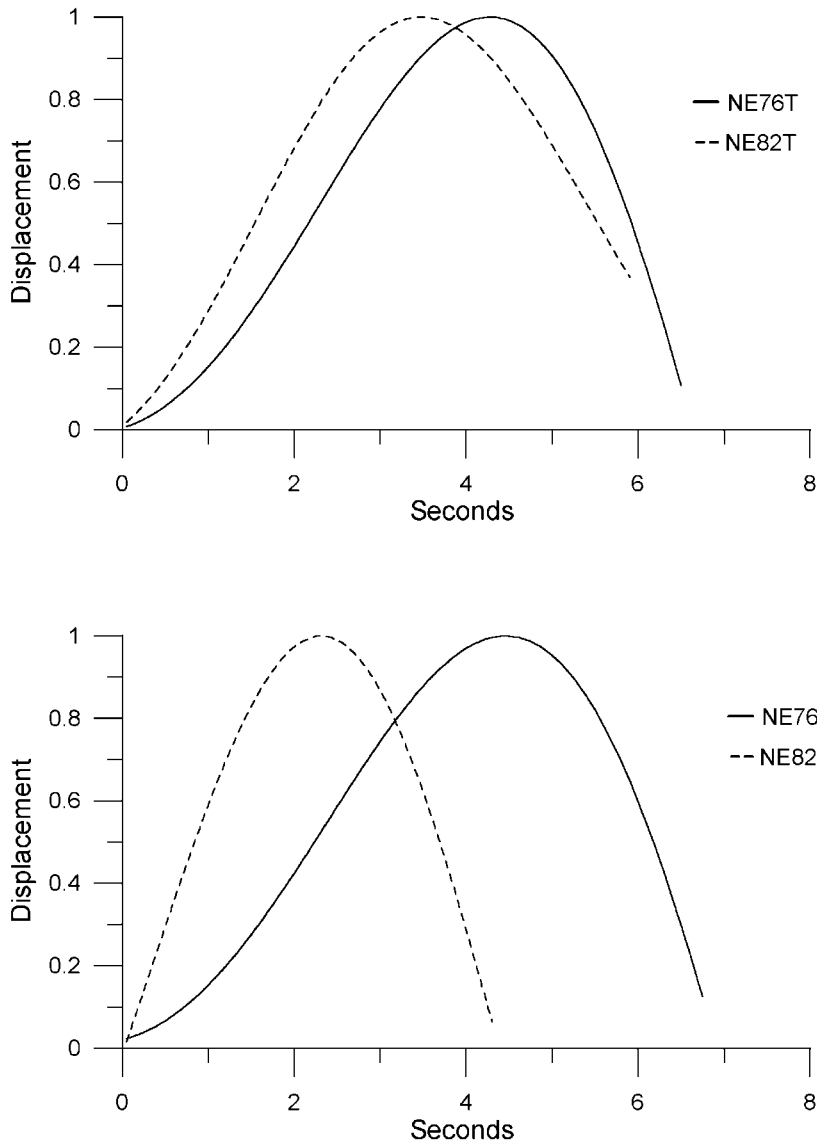| Reference	Latitude (° N)	Longitude (° W)	Magnitude M_w	Strike	Dip	Slip	Depth (km)
NEIC	26.33	−110.64	6.4	117°	77°	166°	10
Harvard	26.63	−110.91	6.3	220°	81°	−9°	15
CICESE	26.61	−111.09	6.2	117° ± 4°	79° ± 2°	168° ± 2°	5 ± 2

Figure 6.   Comparison of the filtered source time functions (radial and transversal) observed at the NE76 (continuous line) and NE82 (discontinuous line) seismic stations to infer the rupture directivity. A short source time function can be observed at the NE82 seismic station located southeast of the epicenter due to the rupture directivity compared with the source time function observed at the NE76 seismic station located northwest of the epicenter.
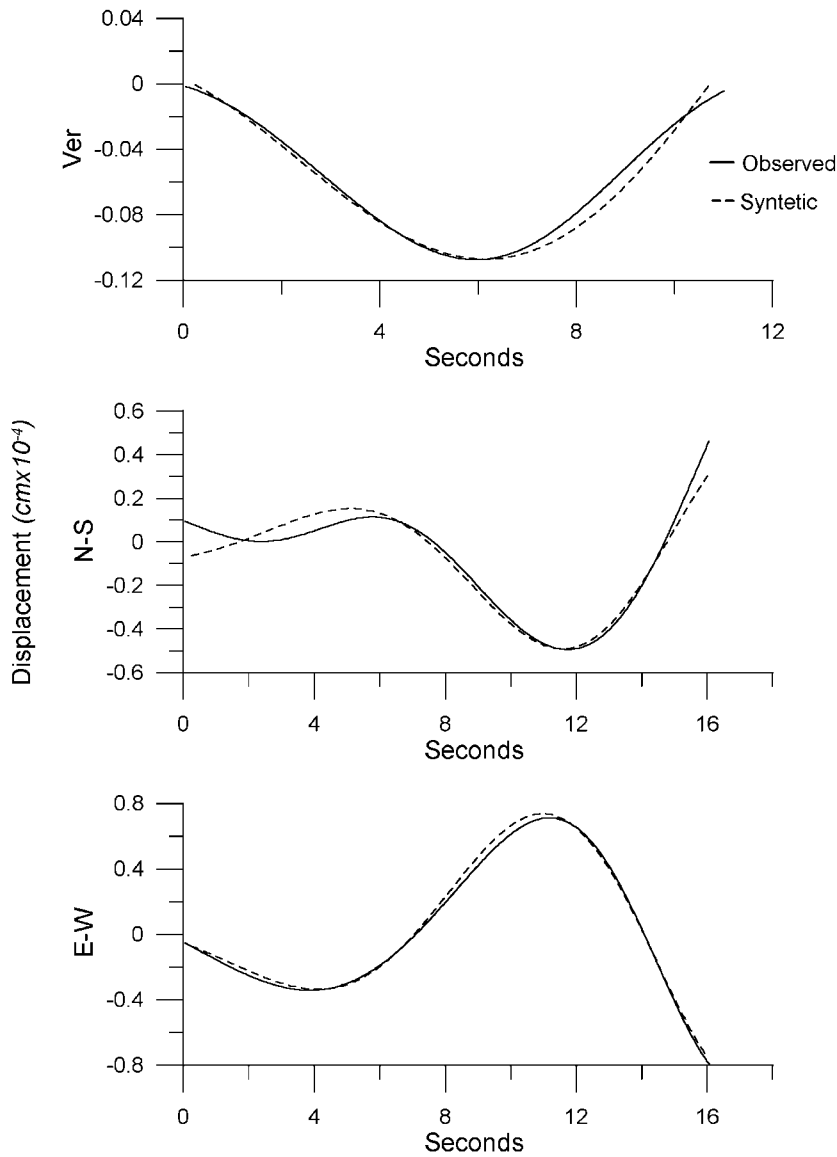
Figure 7.   Comparison of the observed *P*- and *S*-wave amplitudes (continuous line) of the foreshock bandpass filtered between 0.05 and 0.1 Hz recorded at the NE77 seismic station with the synthetic seismograms (discontinuous line) calculated by the reflectivity method (Herrmann, 1987). The fault geometry is the same as the fault geometry of the main event.

synthetic seismograms using a bandpass Butterworth filter between 0.05 and 0.1 Hz. Figure 7 shows the comparison of the synthetic and observed seismograms at NE77. The match is very good. Second, the ASTF of the foreshock recorded at the NE77 and the mainshock recorded at NE76, NE82, and GUYB were normalized and filtered between 0.1 and 0.2 Hz and compared (Fig. 8). It was found that the ASTF of the foreshock and mainshock are similar within the variations due to the directivity effects. We interpreted this result in the following manner. If we assume that both events have the same fault area, the foreshock was a very slow event with a displacement given by

$$u_f = u_m \frac{M_{0f}}{M_{0m}},$$

where u_m is the average displacement of the mainshock, M_{0m} is the seismic moment of the mainshock and M_{0f} is the seis-

mic moment of the foreshock. After the occurrence of the foreshock the same fault area moved again but with a large displacement given by u_m.

Spectral Analysis

We used Brune's (1970) theory to calculate source parameters. A time window of 20 sec was used to calculate displacement spectra of the horizontal records of the NE76 seismic station. Figure 3 shows the used time windows, and Figure 9 shows the displacement spectra. No correction due to seismic attenuation was applied because we observed that the displacement spectra have a ω^{-2} behavior at high frequencies. A corner frequency of 0.18 ± 0.02 Hz was picked (5.5 ± 0.5 sec). Within the errors picks, this corner frequency agrees with the duration of the ASTF obtained with the waveform modeling. Assuming a circular fault (Brune, 1970), the source radius is given by
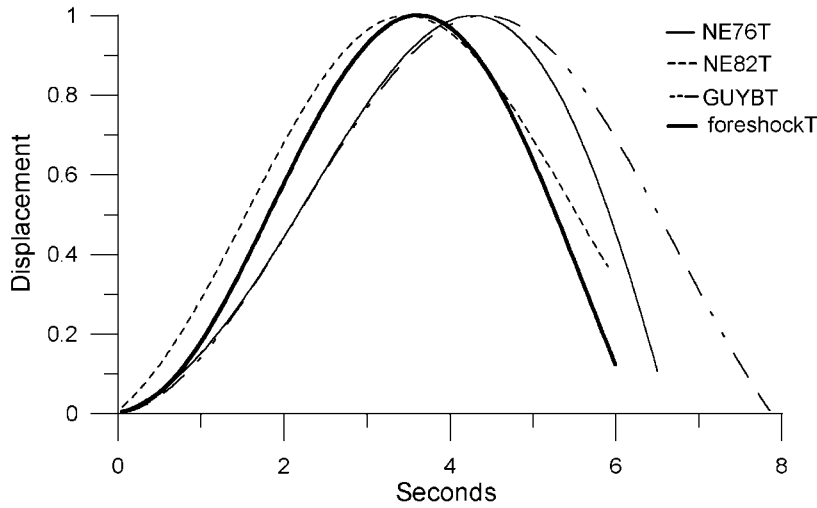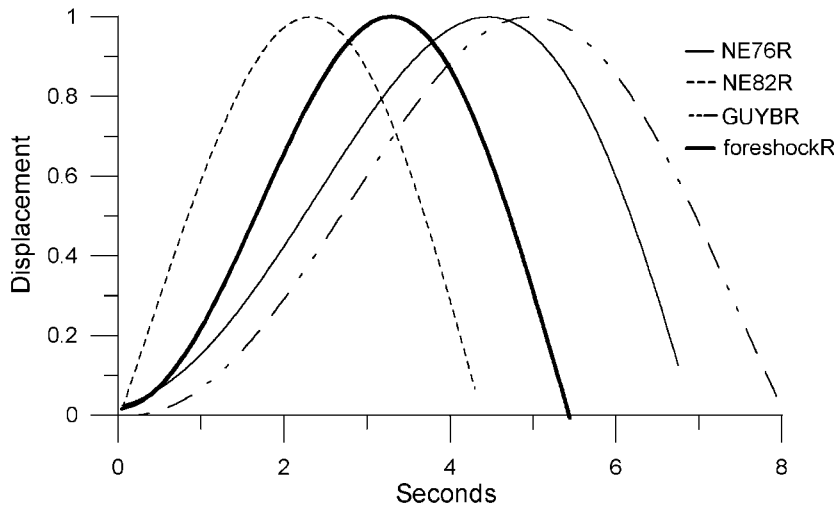
Figure 8. Comparison of the normalized ASTF of the mainshock observed at different azimuths with the ASTF of the foreshock (continuous line) observed at the NE77 seismic station. The ASTFs were rotated and filtered using a bandpass Butterworth filter between 0.1 and 0.2 Hz. R, radial; T, transversal. Note the similarity of the ASTFs.

$$ r \ = \ 0.3724 V_{c0} / f_c \ , $$

where f_c is the corner frequency and V_{c0} is the shear-wave velocity at the source. The source radius can also be calculated by using the duration of the source time function ζ given by $r = 0.3724 V_{c0} \zeta$. To calculate the seismic moment, we used the displacement spectra; we called this spectral seismic moment M_Ω. The seismic moment (M_0) and the seismic moment rate function ($\partial M(t - r/\beta)/\partial t$) were calculated integrating the time domain of the observed *S*-wave pulses at the NE76 seismic station (Table 4). The static stress drop is given by

$$ \Delta\sigma \ = \ (7/16) M_0 / r^3 \ , $$

where M_0 is the seismic moment and r is the source radius. A shear-wave velocity of 3.3 km/sec was used to calculate the static stress drops. To find trends of the stress drops of

events of magnitude greater than 5 that have occurred in the transform faults and spreading centers of the Gulf of California, we calculated the stress drops using the duration of the ASTF of the events reported by Goff *et al.* (1987) and Tanioka and Ruff (1997). The calculated stress drop of the Loreto earthquake using the duration of the ASTF is 3.8 Mp (Table 4). We found that the largest static stress drops are associated with events located in the transform fault that connect the Guaymas and Carmen basins. On the other hand, the ASTF of the Gulf of California events is between 2 and 12 sec. The shape of the ASTFs at the head of the Gulf of California are simple with a triangular shape, probably because the earthquakes are small with magnitudes smaller than 6.0. Toward the mouth of the Gulf of California the magnitudes of the events are greater than 6.0 and the shapes of the ASTFs are complex and trapezoidal. Table 5 shows the duration and shape of the ASTF and the static stress drops of the events studied in the Gulf of California.
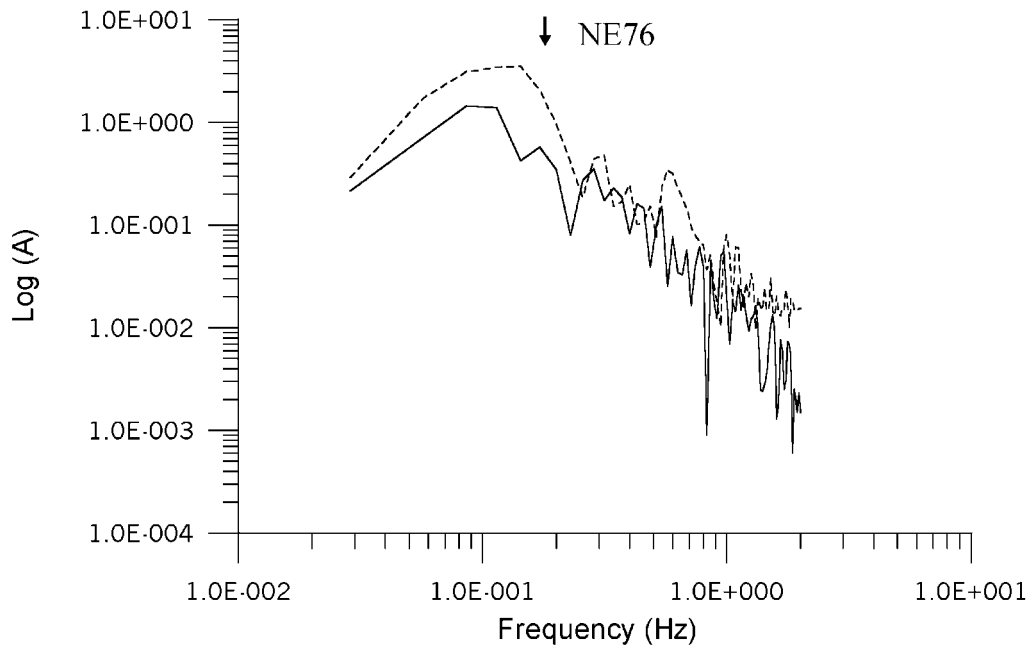
Figure 9. *S*-wave displacement spectra of north–south (continuous line) and east–west (discontinuous line) components of the NE76 seismic station. A time window of 20 sec was used to calculate the spectra. Arrow shows the location of the corner frequency.

Discussion and Conclusion

We located the Loreto earthquake of 12 March 2003 northwest of the Carmen basin at a depth of 5 ± 2 km (Fig. 2). An ASTF with an average duration of 6 sec was observed. Forward waveform modeling of *P* and *S* waves were used to obtain the following fault geometry: strike, $117° \pm 4°$; dip, $79° \pm 2°$; and slip, $168° \pm 2°$. This is a right-hand strike-slip fault that agrees with the inferred transform fault between the Guaymas and Carmen basins. We located a foreshock of magnitude 4.2 in the same area of the main event. The foreshock has an ASTF of 5.5 sec similar to the ASTF of the main event, which suggests that this was a small, very slow event. It was possible to locate only seven aftershocks of the Loreto earthquake with enough precision in the rupture area of the mainshock inferred from the Brune circular fault model (Fig. 2). Other aftershocks were located away of the fault area toward the southeast, which suggests a stress expansion beyond the rupture area.

Waveform analysis showed that the ASTF of the foreshock is similar to the ASTF of the mainshock in shape and duration as well as in its fault geometry. We think that the foreshock initially overcame the prevalent friction forces and the sides of the fault area slipped away with an average displacement of 1000 times less than the average displacement of the magnitude 6.2 mainshock. From the effects of the rupture directivity on the source time function at different azimuths, we were able to infer that the rupture propagated from the northwest to the southeast.

The locations of the 1901 (M_w 7.0) and 1964 (M_w 6.3 and 6.5) events are likely to have occurred in the transform fault that connects the Carmen and Farallon basins. Recently, the stresses were concentrated in zones of high strength (asperities) over the transform fault that connects Carmen and Guaymas Basins and the accumulated stresses have been released with the events of 1971 (M_w 6.5), 1974 (M_w 6.3), 1988 (M_w 6.6), 1995 (M_w 6.0), and 2003 (M_w 6.2). Earthquakes that have occurred in this sector of the Gulf of California have had large static stress drops, probably suggesting the break-up of the crust in a transition zone from oceanic to continental crust (Table 5). We think that it is most likely because of the thinning of the crust between Guaymas and Farallon basins, this area is prone to large events.

We searched for source parameters of events located in the Gulf of California (Goff *et al.*, 1987; Rebollar *et al.*, 2001) to use the duration of the source time function to calculate the static stress drops and to compare them with the calculated stress drop of the Loreto earthquake. The static stress drops of events that have occurred in the Gulf of California range from 2 to 125 bars (Table 5).

Stress drops appear to increase from the northwest to the southeast. The smaller stress drops, however, are due to events that have occurred in the Wagner and Delfin basins and range from 2 to 18 bars. Toward the southeast in the Canal de Ballenas transform fault, located between the Upper Delfin and Salsipuedes basins (Fig. 1), the stress drops increased in the range from 2 to 49 bars. The events with

Table 4
Source Parameters Calculated with the Seismic Records of the NE76 Seismic Station

Seismic Station	r (km)	β (km/sec)	M_0 (dyne cm)	$\partial M/\partial t$ (dyne cm/sec)	M_Ω (dyne cm)	$\Delta\sigma$ (bar)	$\Delta\sigma_\Omega$ (bar)
NE76	6.8 ± 0.7	3.3	2.68×10^{25}	2.04×10^{24}	2.56×10^{25}	38 ± 12	36 ± 12

r is the source radii, β is the shear-wave velocity, M_0 is the seismic moment calculated by integrating in the time domain the observed S waves, $\partial M/\partial t$ is the seismic moment rate, M_Ω is the spectral seismic moment calculated from the displacement spectra, $\Delta\sigma$ is the static stress drop calculated with the duration of the ASTF, and $\Delta\sigma_\Omega$ is the static stress drop calculated with the displacement spectra.

Table 5
Source Parameters of 20 Earthquakes with Magnitudes Greater than 5 That Have Occurred in the Gulf of California

Gulf of California	Earthquake (yyyy/mm/dd)	M_W	M_0 (N m)	Source Time Function	Duration (sec)	Stress Drop (bars)	Depth (km)	Focal Mechanism*
Northern sector								
Wagner basin	1969/03/20	5.7	0.48×10^{18}	Triangular[†]	6	5	6	23/43/273
	1969/03/21	5.6	0.33×10^{18}	Triangular[†]	3.5	18	3	35/43/274
Delfin basin	1997/11/26	5.3	0.12×10^{18}	Triangular[‡]	3	2.2	5	330/85/165
Canal de ballenas	1975/07/08	6.5	5.9×10^{18}	Triple source triangular[†]	12	8	1–7	132/93/170
	1963/11/18	6.4	4.6×10^{18}	Trapezoid-triangular[†]	6	49	7	131/111/167
St Pedro Martir basin	1965/02/27	5.9	1.1×10^{18}	Trapezoidal-triangular[†]	11	2	5	133/48/190
Middle sector								
Guaymas basin	1984/02/10	6.0	1.2×10^{18}	Double source triangular[†]	8	5	6	127/96/182
	1974/05/31	6.3	3.8×10^{18}	~Triangular[†]	12	5	3–5	123/65/169
Carmen basin	2003/03/12	6.2	2.6×10^{18}	Triangular	5.5 ± 0.5	38 ± 12	5.0 ± 2	117/79/168
	1995/08/28	6.2	3.0×10^{18}	Complex[§]	4.4	82	14	222/78/0
	1971/09/30	6.5	6.7×10^{18}	Triangular[†]	5	125	7	128/85/179
	1964/07/05	6.3	4.0×10^{18}	~Trapezoidal[†]	12	5	—	128/58/175
Farallon basin	1964/07/06	6.5	7.8×10^{18}	~Trapezoidal[†]	10	18	3	129/76/175
	1973/03/25	5.7	0.4×10^{18}	Trapezoid[†]	4.5	12	9	153/94/190
South sector								
Escudo continental	1969/04/04	5.9	0.8×10^{18}	Trapezoidal[†]	6	9	9	152/53/163
Pescadero Basin	1975/09/24	6.0	1.6×10^{18}	Trapezoid[†]	6	17	9	129/72/173
	1969/08/17	6.5	6.5×10^{18}	Double-source triangular[†]	10	15	10	129/76/175
Tamayo Fracture Zone	1971/01/19	6.0	1.2×10^{18}	Trapezoidal[†]	6	13	4	127/84/176
	1969/11/01	6.6	11.0×10^{18}	Complex[†]	12	15	6	122/77/175
Tres Marias	1976/02/09	5.8	0.7×10^{18}	Triangular[†]	3	60	11	92/52/86

*Focal mechanisms are given by strike/dip/rake.
[†]Goff *et al.* (1987).
[‡]Rebollar *et al.* (2001).
[§]Tanioka and Ruff (1997).

the largest stress drops are located on the transform faults between the Guaymas and Farallon basins (Table 5). This could indicate that the friction between the plates is not uniform and that in some regions like the transform fault between the Carmen and Guaymas basins, there are strong asperities, so that the events that occur in this zone reach stress drops similar to the static stress drops of intraplate earthquakes, according to the range of values reported by Kanamori and Anderson (1975) and Scholz *et al.* (1986).

Acknowledgments

References

Brune, J. N. (1970). Tectonic stress and the spectra of seismic shear waves from earthquakes, *J. Geophys. Res.* **75,** 4997–5009.

Goff, J. A., E. A. Bergman, and S. C. Solomon (1987). Eathquake source mechanism and transform fault tectonics in the Gulf of California, *J. Geophys. Res.* **92,** 10,485–10,510.

Herrmann, R. B. (1987). *Computer Programs in Seismology*, St. Louis University, St. Louis, Missouri.

Kanamori, H., and D. L. Anderson (1975). Theoretical basis of some empirical relations in seismology, *Bull. Seism. Soc. Am.* **65,** 1073–1095.

Larson, P. A., J. D. Mudie, and R. L. Larson (1972). Magnetic anomalies and fracture-zone trends in the Gulf of California, *Geol. Soc. Am. Bull.* **83,** 3361–3368.

Lienert, B. R., and J. Havskov (1995). A computer program for locating earthquakes both locally and globally, *Seism. Res. Lett.* **66,** 26–36.

Lienert, B. R., E. Berg, and L. N. Frazer (1988). HYPOCENTER: an earthquake location method using centered, scaled, and adaptively least squares, *Bull. Seism. Soc. Am.* **76,** 771–783.

Lomnitz, C., F. Mooser, C. R. Allen, J. N. Brune, and W. Thatcher (1970). Seismicity and tectonics of the northern Gulf of California region: preliminary results, *Geofis. Int.* **10,** 37–48.

Lonsdale, P. L. (1989). Geology and tectonics history of the Gulf of California, in *Geology of North America: The Eastern Pacific Ocean and Hawaii*, Vol. N, Boulder, Colorado, Geological Society of America.

Pacheco, J. F., and L. R. Sykes (1992). Seismic moment catalog of large shallow earthquakes, 1900 to 1989, *Bull. Seism. Soc. Am.* **82,** 1306–1349.

Rebollar, C. J., and M. S. Reichle (1987). Analysis of the seismicity detected in 1982–1984 in the Northern Peninsular ranges of Baja California, *Bull. Seism. Soc. Am.* **77,** 173–183.

Rebollar, C. J., L. Quintanar, R. Castro, S. Day, J. Madrid, J. N. Brune, L. Astiz, and F. Vernon (2001). Source characteristics of a 5.5 magnitude earthquake ocurred in the transform fault system of the Delfín Basin in the Gulf of California, *Bull. Seism. Soc. Am.* **91,** 781–791.

Reichle, M., and I. Reid (1977). Detailed study of earthquake swarms from the Gulf of California, *Bull. Seism. Soc. Am.* **67,** 159–171.

Scholz, C. (1968). The frequency-magnitude relation of microfracturing in rock and its relation to earthquakes, *Bull. Seism. Soc. Am.* **58,** 399–415.

Scholz, C. H., C. A. Aviles, and S. G. Wesnousky (1986). Scaling differences between large interplate and intraplate earthquakes, *Bull. Seism. Soc. Am.* **76,** 65–70.

Tanioka, Y., and L. Ruff (1997). Source time functions, *Seism. Res. Lett.* **68,** 386–400.

Trampert, J., H. Paulssen, A. van Wettum, J. Ritsema, R. Clayton, R. Castro, C. J. Rebollar, and A. Perez-Vertti (2003). New array monitors seismic activity near the Gulf of California in Mexico, *EOS* **84,** no. 4, 29–32.

Centro de Investigación Científica y de Educación Superior de Ensenada
Departamento de Sismología
Km 107 Carretera Tijuana-Ensenada
Ensenada, Baja California, Mexico CP 22860